On the effect of sea drops on the atmospheric boundary layer

Vladimir N. Kudryavtsev[1,2]

Received 24 March 2005; revised 7 April 2006; accepted 28 April 2006; published 22 July 2006.

[1] One of the possible mechanisms responsible for the reduction of the sea surface drag at high winds is explored. The mechanism is based on the direct effect of sea drops (as heavy particles) on the turbulent mixing. If assumed that sea drops are ejected upward from the sea surface, no significant effect can be found. A more realistic picture presumes that the spume drops (resulting from a mechanical tearing of wave crests) are ejected "horizontally" at altitudes of breaking crests. A model of the spume drops generation is proposed. The spume drops, being torn off from breaking crests and sprayed inside the airflow, significantly affect the surface drag. At highest model wind speeds (60–80 m/s) the model actually predicts an effect of the "slippery surface" when the drag coefficient is reduced in about 10 times. A comparison with available observations is given.

Citation: Kudryavtsev, V. N. (2006), On the effect of sea drops on the atmospheric boundary layer, *J. Geophys. Res.*, *111*, C07020, doi:10.1029/2005JC002970.

1. Introduction

[2] Recently, the experimental evidence of the saturation of the surface drag at high (hurricane) wind speeds was reported. *Powell et al.* [2003] measured the wind velocity profiles in the tropical cyclone, and found that the neutral stability drag coefficient were leveled off and then dropped as the wind speed increases above the hurricane force. As noted, this behavior contradicts to the parameterizations which are currently used in the hurricane and storm surge modeling. Revealed reduction of the drag coefficient is supported by estimates of the angular momentum budget and the frictional dissipation made by *Kaplan and Frank* [1993]. Sensitivity studies of the tropical cyclone models performed by *Emanuel* [1995] showed that cyclones cannot attain their observed intensity with traditional parameterizations of the drag coefficient, and it is necessary to reduce the drag. He argued that at hurricane winds the ratio of enthalpy to momentum exchange coefficient to be in the range 1.2–1.5 that twice exceeds the "normal" value. This leads to a speculation that at hurricane wind conditions the sea drag coefficient should be in 4-times reduced in respect to a "standard" parameterizations. *Andreas and Emanuel* [2001] were the first who incorporated effect of spray into a tropical cyclone model, and showed that at hurricane force winds the spray-induced enthalpy flux is very significant, more than enough to offset the increased surface drag.

[3] *Donelan et al.* [2004] investigated the aerodynamic roughness of the water surface at extreme winds in the laboratory conditions. They observed a saturation of the surface drag at the wind speed exceeding 33 m/s. As a plausible mechanism, the separation of the airflow from continually breaking crests was suggested.

[4] Saturation of the surface stress at increasing high winds is implicitly supported by the scatterometer measurements. Data by *Donnely et al.* [1999] on C-band ocean backscatter at high wind conditions clearly showed a saturation of the backscatter power at wind speeds exceeding 25 m/s. A similar effect was found by *Donelan et al.* [2004] in the laboratory conditions. Relation of the surface "roughness" (which scatters radio waves) to the wind surface stress is not obvious. However, if such relation does exist, the saturation of the backscatter at high winds presumes decreasing of the surface drag coefficient.

[5] Recently, *Andreas* [2004] and *Makin* [2005] proposed two different model approaches to estimate effect of the sea drops on the wind stress. *Makin* [2005] suggested that at high wind speeds (>35 m/s), a thin (with thickness of about 10% of significant wave height) atmospheric boundary layer adjacent the surface turns to a regime of limited saturation by suspended sea drops. At this regime the Richardson number of this layer reaches the critical value that results in a reduction of the surface drag and acceleration of the airflow. However, no argumentation on validity of this regime for the real rate of the sea spray production (e.g., as predicted by *Andreas* [1998]) had been done. On the contrary, *Andreas* [2004] ignored effect of the sea spray on the atmospheric stratification, and focused on their impact on the momentum balance in the atmospheric boundary layer. He suggested that once created, sea drops are accelerated to the wind speed, and thus redistribute the stress in the near surface atmosphere. As found, at wind speed of 30 m/s and less effect of sea drops on momentum

[1]Nansen International Environmental and Remote Sensing Center (NIERSC), Saint-Petersburg, Russia.
[2]Also at Nansen Environmental and Remote Sensing Center (NERSC), Bergen, Norway.

0148-0227/06/2005JC002970

flux in the atmospheric boundary layer is negligible. However, due to strong wind dependence of the sea drops production, their impact rapidly increases, and at wind speed of 60 m/s the sea drops dominate momentum balance and affect the sea surface drag.

[6] In the present paper we explore a mechanism of the direct impact of the sea drops (as heavy particles) on marine atmospheric boundary layer through the buoyancy forces that influence the turbulence kinetic energy and turbulent mixing. In that sense, considering mechanism is similar to that occur in the dust storms, or/and to the suspension of mixed-sized gravel and sand in water in a turbidity current. Entrainment of dust from the surface into the atmospheric boundary layer damps the turbulent mixing (similar to the effect of the stable thermal stratification) and results in acceleration of the airflow (see, e.g., *Barenblat and Golitsyn* [1974] and their references for the dust storms, and *Bagnold* [1962] for a turbidity current). With some modifications the model approach proposed by *Barenblat and Golitsyn* [1974] is adopted in the present study. As far as possible, the model calculations presented here are based on empirical estimates on the rate of sea drops production which are systematized and given by *Andreas* [1998]. Our analysis is limited to the case when mass of the drops is small in comparison with the air one. Therefore effect of sea drops on momentum balance (considered by *Andreas* [2004]) is omitted.

[7] The paper is organized as the following. In section 2 we describe the governing equations. Effect of sea spray at a "natural" assumption that they are ejected upward at the sea surface is considered in section 3. In section 4 we further develop a model of generation of spume drops (as shown in section 3 the role of bubble drops is weak) and their impact on the atmospheric boundary layer and the surface drag. Model calculations and comparison with available data are presented in section 5. In section 6 we discuss what model does predict if production of spume drops and their vertical distribution are imposed empirically. Conclusion is given in section 7.

2. Governing Equation

[8] Sea droplets are ejected into the Marine Atmospheric Boundary Layer (MABL) by means of two basic mechanisms: bursting of the air bubbles (generated by the wave breaking) at the sea surface, - bubble droplets, and the wind tearing of wave crests, - spume droplets (see, e.g., review by *Andreas* [1998]). Once ejected into the airflow, the sea droplets (depending on their size) may be either fallen down to the surface or transported upward by the turbulence. Though the volume concentration of the sea droplets normally is small, water density (density of an individual droplet) is much larger the air one. Thus, following the analogy with the dust storm, we may anticipate an impact of sea droplets on MABL dynamics.

[9] The present study is based on the model for the turbulent flow with suspended heavy particles proposed earlier by *Barenblat* [1953], *Kolmogorov* [1954], and described in more complete form by *Monin and Yaglom* [1965] and by [*Barenblat and Golitsyn*, 1974]. Governing equations accounting for effects of both thermal stratification and heavy suspended particles are [*Barenblat and Golitsyn*, 1974]:

$$\mathrm{k}u_z = u_*^2 \tag{1}$$

$$\mathrm{k}\theta_z = -q \tag{2}$$

$$\mathrm{k}s_z = -as + I_s \tag{3}$$

$$\mathrm{k}u_z^2(1 - Ri - Ko) - diss = 0 \tag{4}$$

$$Ri = (g/\theta_0)\theta_z/u_z^2 \tag{5}$$

$$Ko = -\sigma g s_z/u_z^2 \tag{6}$$

where subscript z at any quantity y denotes its partial derivative over z ($y_z \equiv \partial y/\partial z$); u, θ, s are the wind velocity, potential temperature and concentration of droplets correspondingly; u_* and q are the friction velocity and kinematic heat flux; I_s is a volume source/sink of droplets; k is the turbulent eddy viscosity coefficient, which is assumed to be the same for any quantity; *diss* is the turbulent kinetic energy (TKE) dissipation; *Ri* and *Ko* are the Richardson and the Kolmogorov numbers; g is the gravity acceleration; θ_0 is the characteristic air temperature in °K; $\sigma = (\rho_w - \rho_a)/\bar{\rho}$ is a relative excess of the sea droplets density ρ_w over the air density ρ_a; $\bar{\rho}$ is the mean density; a is the terminal fall velocity of the droplets defined by the Stokes relation

$$a(r) = \frac{2}{9}\frac{\rho_w}{\rho_a}\frac{gr^2}{\nu_a} \tag{7}$$

r is droplet radius (which is assumed much smaller than the turbulent scale); ν_a is kinematic coefficient of the air molecular viscosity.

[10] Equations (1)–(6) are written in the Boussinesq approximation. This presumes that variation of the air and sea spray mixture density in respect to the air one is small, i.e. $s\sigma \ll 1$, and thus sea drops can affect the MABL dynamics through the action of the buoyancy force only. For the same reason, impact of sea drops on momentum balance (1) (so called spray stress considered by *Andreas* [2004]) is omitted. Also, in order to focus on the direct effect of sea drops on MABL, their impact on the heat balance (2) by means of the latent heat flux from the spray surface is omitted. This problem was studied in detail by, e.g., *Andreas et al.* [1995] and *Makin* [1998]. Notice, that unlike the model by *Barenblat and Golitsyn* [1974], we have introduced a volume source/sink of droplets I_s in the spray conservation equation (3). This source may model, e.g., a decrease of s due to evolution of drops in size at evaporation, or generation of spume droplets, which are torn off from wave crests and ejected into the airflow at some altitude. The latter is considered below, in section 4.1.

[11] Originally equations (1)–(6) were derived for the stationary Cartesian coordinate system, and their use for the

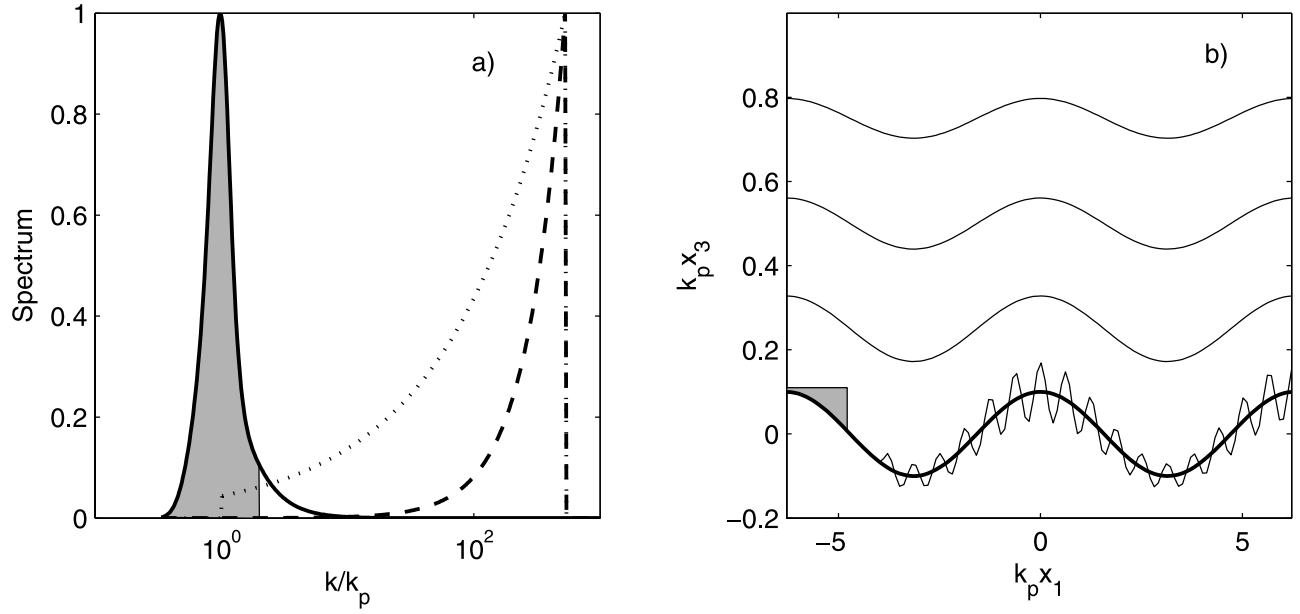

Figure 1. (a) Spectra of the sea surface displacement [*Donelan et al.*, 1985] (solid line; wave age 1.5), and white caps coverage (dotted line) and length of wave breaking fronts (dash line) [*Phillips*, 1985] normalized on their peak values. Shaded area indicates spectral interval $k < 2k_p$, where k_p is the spectral peak wavenumber. (b) Sketch of the sea surface which is represented as a superposition of dominant waves (thick line), modulated shorter waves and a breaking crest of a dominant wave (shaded triangle). Thin solid lines above are coordinate lines $z = const$ (8) following smooth dominant waves.

wave boundary layer should be argued. Production of bubble and spume drops are normally associated with the wave breaking events. Rate of generation of bubble drops is proportional to the white caps coverage (q_b) [*Andreas*, 1998], while generation of spume drops - to the length of wave breaking crests (L_b) (e.g., *Anguelova et al.* [1999] and section 4.1). *Phillips* [1985] argued that the main contribution to these quantities comes from breaking of shortest waves, and quantities q and L_b are proportional to $q_b \propto u_*^3 g^{-3/2} \int k^{1/2} dk$ and $L_b \propto u_*^3 g^{-3/2} \int k^{3/2} dk$. Spectral density of q_b and L_b normalized on their peak values are shown in Figure 1a. Empirical wavenumber spectrum by *Donelan et al.* [1985] of the sea surface displacement for inverse wave age 1.5 (at high wind conditions wind waves are apparently not mature) normalized on its peak value is also shown. As it follows from this figure, wind waves that generate sea drops and that provide the main vertical displacement of the surface are strongly separated in k-space. This presumes that fixed Cartesian coordinate system cannot be used due to apparent difficulties with an averaging of the governing equations between crest and troughs of the energy containing wave. Spectrum of real wind seas is quite narrow (see Figure 1a), and in the range of inverse wave age from 1 to 2 the wind waves with $k < 2k_p$ and $k < 3/2k_p$ contain about 80% and 65% of the total sea surface variance (σ_ζ^2) or about 90% and 80% of its total std.dev.(σ_ζ) correspondingly. Moreover, in the mean the slope of these waves is small, $\sigma_\zeta k_p \simeq 0.05$, thus they can be treated as waves of a "small amplitude". Hereinafter we introduce the coordinate system following the energy containing waves, which may be defined (for concreteness) as waves with $k = k_p \pm 1/2k_p$. This coordinate system follows a "smooth" sea surface, with filtered out higher frequency waves including superharmonics of the dominant waves. Coordinate systems following the dominant waves are normally used in sea spray studies (see, e.g., review by *Andreas et al.* [1995]).

[12] The conformal mapping proposed by *Benjamin* [1959] is the most suitable for study of shearing flow over a wavy boundary (see, e.g., direct numerical simulations by *Sullivan et al.* [2000]). If x_1 and x_3 are the Cartesian coordinates, the "upward" component z of the coordinate system following a wave with amplitude A, wavenumber K and frequency Ω is defined as

$$z = x_3 - Ae^{-Kx_3} \cos(Kx_1 - \Omega t) \tag{8}$$

As shown, e.g., by *Kudryavtsev and Makin* [2004, equations (A12) and (A18)], in the case of a quasi-monochromatic surface wave, the momentum and TKE conservation equations written in the wave-following orthogonal coordinate system proposed by *Benjamin* [1959], and then averaged over the wavelength are similar to that in the Gartesian coordinate system. It is easy to show that in this coordinate system the averaged equations for the stratified turbulent boundary layer are also similar to (1)–(6), if correction of the drops fall velocity a in the second order on the wave slope is ignored.

[13] Notice that in the field of real waves, amplitude A in (8) is not a constant, but is varying function in space and time. For the *Donelan et al.* [1985] spectrum restricted by the interval $k = k_p \pm 1/2k_p$, the mean number of waves in wave groups (as defined by *Longuet-Higgins* [1957]) is

about 4.5. It means that in the coordinate system moving with the phase speed, time scale of local amplitude variability in 10-times exceeds the wave period, i.e. A is a slowly varying function. This may justify validity of the comformal mapping of the governing equations for the real conditions.

[14] Thus we consider the coordinate system following the "smooth" surface formed by dominant waves with $k < 3/2k_p$. The shorter wind waves and super-harmonics of the dominant waves are superimposed on the smooth surface as shown schematically in Figure 1b. Definition of smooth surface does not presume its breaking. As found by *Longuet-Higgins* [1978], breaking of the dominant wave crests results from strong hydrodynamic instability of super-harmonics, which are excluded from the definition of the "smooth" surface. The tail of wave spectrum, through wave-induced momentum flux and airflow separations from breaking crests, supports the major part of the form drag [see, e.g., *Kudryavtsev and Makin*, 2001]. Besides, one may anticipate that a major part of sea drops is also produced by these waves (see Figure 1a). Thus, after averaging over the scales of dominant waves, the shorter wind waves (including super-harmonics of dominant waves) can be parameterized through an aerodynamic roughness scale of the smoothed surface, z_0, and a spray generation function (and/or volume source of drops generation I_s in (3)). Note also that dominant waves strongly modulate breaking of the shorter waves [*Dulov et al.*, 2002]. Therefore almost all of wave breaking events occur on the crests of dominant waves, and acceleration of the airflow over these crests provide auspicious conditions for the sea drops generation.

[15] Thus hereinafter we consider equations (1)–(6) as equations written in the coordinate system following the smoothed dominant surface waves, and averaged over their scales. The vertical coordinate z counts off the wavy surface, and $z \geq z_0$. In these equations the shorter waves are parameterized through a source of sea drops I_s, and an aerodynamic roughness scale z_0. When solution of equations (1)–(6) is found, any quantity $Y(z)$ can be transformed to the mean quantity in the "regular" fixed Cartesian coordinate system as $Y(x_3) = \overline{Y(z(x_3))}$, where bar over Y means averaging over z at $x_3 = const$ which are linked by (8) with wavenumber corresponding to the spectral peak wavenumber and amplitude $A \simeq \sqrt{2}\sigma_\zeta$.

[16] As in the work of *Barenblat and Golitsyn* [1974], the following closure for (1)–(6) are adopted:

$$\mathrm{k} = le^{1/2} \tag{9}$$

$$diss = e^{3/2}l^{-1} \tag{10}$$

$$l = \kappa z \Phi(B) \tag{11}$$

where e is the TKE; l is the turbulent mixing length; κ is the von Karman constant; Φ is a mixing length function of the buoyancy parameter $B = Ri + Ko$. Notice, that diss is written with an accuracy to a universal constant, which for the sake of simplicity is included in e. With use of (9)–(11), equations (1)–(6) are reduced to:

$$e = u_*^2(1-B)^{1/2} \tag{12}$$

$$\frac{\partial s}{\partial z} = -\omega\left(s - s_*\right)\frac{\kappa}{u_*}\frac{\partial u}{\partial z} \tag{13}$$

$$\frac{\partial u}{\partial z} = \frac{u_*}{\kappa z}(1-B)^{-1/4}\Phi^{-1}(B) \tag{14}$$

where $\omega = a/(\kappa u_*)$ is the dimensionless falling velocity, $s_* = I_s/a$ is an integral volume source of droplets normalized on a.

[17] To define the mixing length function Φ we note that thermal and sea drops effects appear in equations (12)–(14) additively. Therefore, function Φ can be determined through the Monin-Obukhov (MO) similarity theory for the temperature stratified boundary layer. Within the frame of this theory the wind velocity gradient is

$$\frac{\partial u}{\partial z} = \frac{u_*}{\kappa z}\varphi(z/L) \tag{15}$$

where $L = -(\theta_0/g)u_*^3/(\kappa q)$ is the MO length scale. For the stably stratified boundary layer function φ reads

$$\varphi(\varsigma) = 1 + b\varsigma \tag{16}$$

where $\varsigma = z/L$, and b is an empirical constant normally taken as $b = 5$. Substituting (15) in (5), we see that function φ and the Richardson number Ri are linked as

$$Ri = \varsigma/\varphi(\varsigma) \tag{17}$$

At large $\varsigma \gg 1$ the Richardson number is limited to a critical value $Ri_{cr} = 1/b$. If $Ko = 0$ (there are no droplets) equation (14) must be consistent with (15). Thus with the use of (17) function Φ reads

$$\Phi(Ri) = \frac{1 - Ri/Ri_{cr}}{(1-Ri)^{1/4}} \simeq 1 - Ri/Ri_{cr} \tag{18}$$

where the second expression takes into account that at $0 < Ri < Ri_{cr}$ denominator $(1-Ri)^{1/4}$ is between 0.95 and 1, and further is replaced by 1.

[18] As mentioned, Ri and Ko appear in equations (12)–(14) additively. Thus, Φ must be of the same form (18) independently on whether the buoyancy is forced by the thermal or drops factor, or by both factors. Hereinafter we are focusing on the effect of sea drops only. Then, similar to (18), the turbulent mixing length function in the presence of droplets is

$$\Phi(Ko) = 1 - Ko/Ko_{cr} \tag{19}$$

where $Ko_{cr} = 1/b$ is the critical value of the Kolmogorov number. With the use of (19) and definition (6) the

Kolmogorov number Ko relates to parameters of the boundary layer as:

$$Ko = \frac{z/L_s}{1 + bz/L_s} \tag{20}$$

where L_s is the parameter of stratification (with a dimension of the length):

$$\frac{1}{L_s(z)} = \kappa^2 \omega \sigma \left(s - s_*\right) \frac{g}{u_*^2} \tag{21}$$

Parameter L_s is similar to the MO length scale L. However, unlike L, the length scale L_s depends on the height (via $s(z)$ and $s_*(z)$), and may be called as the local length scale. With the use of equations (19)–(21), the wind velocity gradient (14) now reads

$$\frac{\partial u}{\partial z} = \frac{u_*}{\kappa z}\left[1 + b\frac{z}{L_s(z)}\right] \tag{22}$$

This equation together with (13) are the main equations of the present study. The surface boundary conditions for these equations are defined at the height corresponding to the roughness length scale z_0. In the present study (focusing on the effect of spray only), we simply prescribe z_0 by the Charnok relation

$$z_0 = c_0 u_*^2/g \tag{23}$$

with $c_0 = 1.5 \cdot 10^{-2}$. Since we work in the coordinate system following the smooth dominant waves, z_0 parameterizes the aerodynamic roughness supported by the shorter waves. As shown by *Kudryavtsev and Makin* [2001], at wind speeds <25 m/s the Charnok relation quite well parameterizes aerodynamic roughness of the sea surface which is defined by the wave-induced momentum flux and the airflow separations. However, at high wind conditions additional mechanisms, like impact of the foam or effect of the airflow separations from continuous breaking waves, as suggested by *Donelan et al.* [2004] [see also *Kudryavtsev and Makin*, 2001, equations (11) and (12)], can modify the aerodynamic roughness and thus affect the following results.

3. Effect of Spray: Ejection at the Surface

[19] In this section, we assume that ejection of sea droplets into the airflow results from the upward flux at the surface (similar to the dust storms considered by *Barenblat and Golitsyn* [1974]). Thus the integral volume source s_* in (13) is omitted for the time being. At $z = z_0$ the wind velocity is zero, $u(z_0) = 0$ and the upward flux F_0 of droplets of radius r is assumed known. We shall relate this flux to the spray generation function (SGF) which normally is available from the measurements (see review by *Andreas* [1998]. Dimension of F_0 is $[F_0] = \mathrm{m}^3/\mathrm{m}^2/\mathrm{sec}$ and it describes the rate of production of the droplets volume at the unit surface.

[20] Solutions of equations (13) (at $s_* \equiv 0$) and (22) are

$$s(z) = \frac{F_0}{a}\exp\left[-\omega\frac{\kappa u(z)}{u_*}\right] \tag{24}$$

$$u(z) = \frac{u_*}{\kappa}\left[\ln(z/z_0) + b\int_{z_0}^{z} L_s^{-1}(z)dz\right] \tag{25}$$

with L_s defined by (21).

3.1. Asymptotic Behavior

[21] First we consider an asymptotic behavior of (24)–(25) at $z/L_s \ll 1$. This takes place at small z or/and at a rather small concentration of sea droplets. In this case the solution of (24)–(25) is

$$u(z) \simeq \frac{u_*}{\kappa}\ln(z/z_0) \tag{26}$$

$$s(z) \simeq s_0(z_0/z)^{\omega} \tag{27}$$

where $s_0 = F_0/a$ is the surface concentration. This solution is well known, and was obtained by *Prandtl* [1949]. At this condition the stratification parameter z/L_s varies with height as

$$\frac{z}{L_s} = \frac{z_0}{L_{s0}}\left(\frac{z_0}{z}\right)^{(\omega-1)} \tag{28}$$

where L_{s0} is the length scale based on the surface flux of the droplets:

$$\frac{1}{L_{s0}} = \frac{\kappa g \sigma F_0}{u_*^3} \tag{29}$$

At $\omega > 1$ (relatively large particles) parameter z/L_s is a decreasing function of z. Thus solutions (26)–(27) are valid at any height. On the other hand, for small droplets with $\omega < 1$, parameter z/L_s is an increasing function of z, and one may anticipate that at a large height, $z \gg L_{s0}$, the solution (26)–(27) loses its validity.

[22] At $z \gg L_{s0}$ and $\omega < 1$ the vertical gradients of the wind velocity and the droplets concentration (described by (22) and (13) at $s_* \equiv 0$) are reduced to

$$\frac{\partial u}{\partial z} \simeq Ko_{cr}^{-1}\frac{u_*}{\kappa L_s} \tag{30}$$

$$\frac{\partial s}{\partial z} \simeq -Ko_{cr}^{-1}\frac{\omega s}{L_s} \tag{31}$$

Substituting (21) in (31), we obtain the following profile for $s(z)$ at large z, $z \gg L_{s0}$:

$$s(z) \simeq \frac{Ko_{cr}}{\kappa^2 \sigma \omega^2}\cdot\frac{u_*^2}{gz} \tag{32}$$

With the use of this equation, the length scale (21) and the velocity gradient (30) are:

$$L_s = \omega z / Ko_{cr} \tag{33}$$

$$\frac{\partial u}{\partial z} = \frac{u_*}{\omega \kappa z} \tag{34}$$

The latter equation gives the following wind velocity profile:

$$u(z) = \frac{u_*}{\kappa \omega} \ln(z) + \text{const} \tag{35}$$

As well as at small heights ($z \ll L_{s0}$), the wind profile at large z has a logarithmic shape. However, unlike (26) the von Karman constant in this case is multiplied by factor $\omega < 1$, i.e., the wind velocity gradient is larger. It is worthy to note that the droplets profile (32) and the velocity gradient (34) far from the surface does not depend on the surface flux of droplets, i.e., dynamics of the airflow obeys a self-regulation law. It is easy to check that in this regime the Kolmogorov number (6) with (32) and (35) is equal to its critical value Ko_{cr}.

[23] Equations (35) and (32) were first derived by *Barenblat* [1953] [see also *Barenblat and Golitsyn*, 1974] from rather different arguments. He found these solutions from the analysis of the general properties of equations (1)–(6) for such asymptotic regime when at $\omega < 1$ the storage of droplets (dust in his case) at the surface is unlimited. *Barenblat* [1953] called this regime a saturated flow. As it follows from the present analysis, the regime of the saturated flow (described by (35) and (32)) does not inevitably require the unlimited storage and can be realized far from the surface, at $z \gg L_{s0}$. Since the scale L_{s0} depends on F_0, one may expect that at a strong droplets production, the saturated flow may go down to the surface. Nevertheless, at large F_0 the droplets concentration attains relatively large values, and the governing equations (1)–(6) may lose their validity which requires both s and $s\sigma$ to be small: $s \ll 1$ and $s\sigma \ll 1$.

3.2. Impact of "Real" Sea Spray

[24] Let us consider predictions of equations (25), (24) with (21) for the real sea conditions associated with an empirical SGF. It is accepted that sea droplets are basically generated by the air bubbles bursting at the surface (bubble droplets), and by means of tearing off of drops from breaking wave crests (spume droplets). The latter are the largest droplets. Production of droplets are described by the "spectral" SGF which gives the droplets volume flux from the unit surface per unit droplets radius interval. A comprehensive review of empirical SGF is given by *Andreas* [1998]. Based on previous investigations, he proposed an expression for the SGF, adopting existing empirical knowledge. However, the question on what height empirical SGF should be applied to, is still open. In this section, as a first guess, we suggest that F_0 is equivalent to the SGF, that explicitly presumes that all type of sea drops (both bubble and spume) are ejected upward from the sea surface.

[25] Examples of the spectral SGF dF_0/dr for 10-m wind speeds from 10 m/s to 35 m/s are shown in Figure 2a. As discussed by *Andreas* [1998], droplets with a radius $r < 20$ μm are the bubble droplets, while the larger one are the spume droplets. We shall consider integral characteristics of these droplets, their mean radius r_m and the surface flux F_0 defined as

$$r_m = \int r(dF_0/dr)dr \Big/ \int (dF_0/dr)dr \tag{36}$$

$$F_0 = \int (dF_0/dr)dr \tag{37}$$

where for the bubble droplets the limit of integration is $r < 20$ μm, and for the spume droplets is $r > 20$ μm. The mean radius for the bubble and spume droplets correspondingly are $r_m^b = 15$ μm and $r_m^s = 180$ μm, and they are almost wind independent. Figure 2b shows the dependence of SGF for the bubble F_0^b and spume F_0^s droplets versus the friction velocity. The wind dependence of F_0^b is close to u_*^3, that is consistent with wind dependence of the white caps coverage. Generation of spume droplets is stronger and in the mean it is proportional to u_*^4, though a trend to stronger wind dependence is visible at largest u_*.

[26] The dimensionless fall velocity $\omega = a/(\kappa u_*)$ for the bubble ω_b and spume ω_s droplets are shown in Figure 2c. As it follows from this plot, $\omega_b \ll 1$. Therefore the bubble droplets (according to (27)) are distributed over the whole MABL, and may affect its dynamics if F_0^b is large enough. On the other hand, $\omega_s > 1$, and thus spume droplets are too heavy to be transported upward by the turbulence. The length scale L_{s0} (defined by (29)) calculated for the sum of bubble and spume SGF is shown in Figure 2d. Important conclusion is that the stratification length scale L_{s0} is quite large and depending on u_* varies from 300 to 2000 m. As discussed above, in this case the regime of the saturated flow may be realized at very large altitudes ($z > L_{s0}$), and the effect of drops on the main domain of the MABL is weak. In this case spray concentration and wind velocity profiles are given by equations (27) and (26).

[27] To explore this in more detail, we fixed wind speed u_h (as an external parameter) at a reference level h_r, and solved equations (24), (25) with (38) numerically by iterations for the empirical SGF shown in Figure 2. Assuming that h_r belongs to the log-boundary layer, the resistance law (relating the surface wind stress to u_h) follows from (25) and reads

$$C_{dh}^{1/2} \equiv \frac{u_*}{u_h} = \kappa \left[\ln(h/z_0) + b \int_{z_0}^{h} L_s^{-1} dz \right]^{-1} \tag{38}$$

In order to check the effect of sea drops on the main body of the MABL, the reference level was chosen as $h_r = 10^3$m. Certainly, at moderate winds this level belongs to the Ekman part of the planetary MABL, where equations (24) and (25) are not valid. However, we tolerate this inaccuracy (as well as the use of *Andreas*'s [1998] SGF at $u_{10} > 32$ m/s) because these calculations, in fact, perform just for an illustrative purpose. Model calculations for the SGF shown

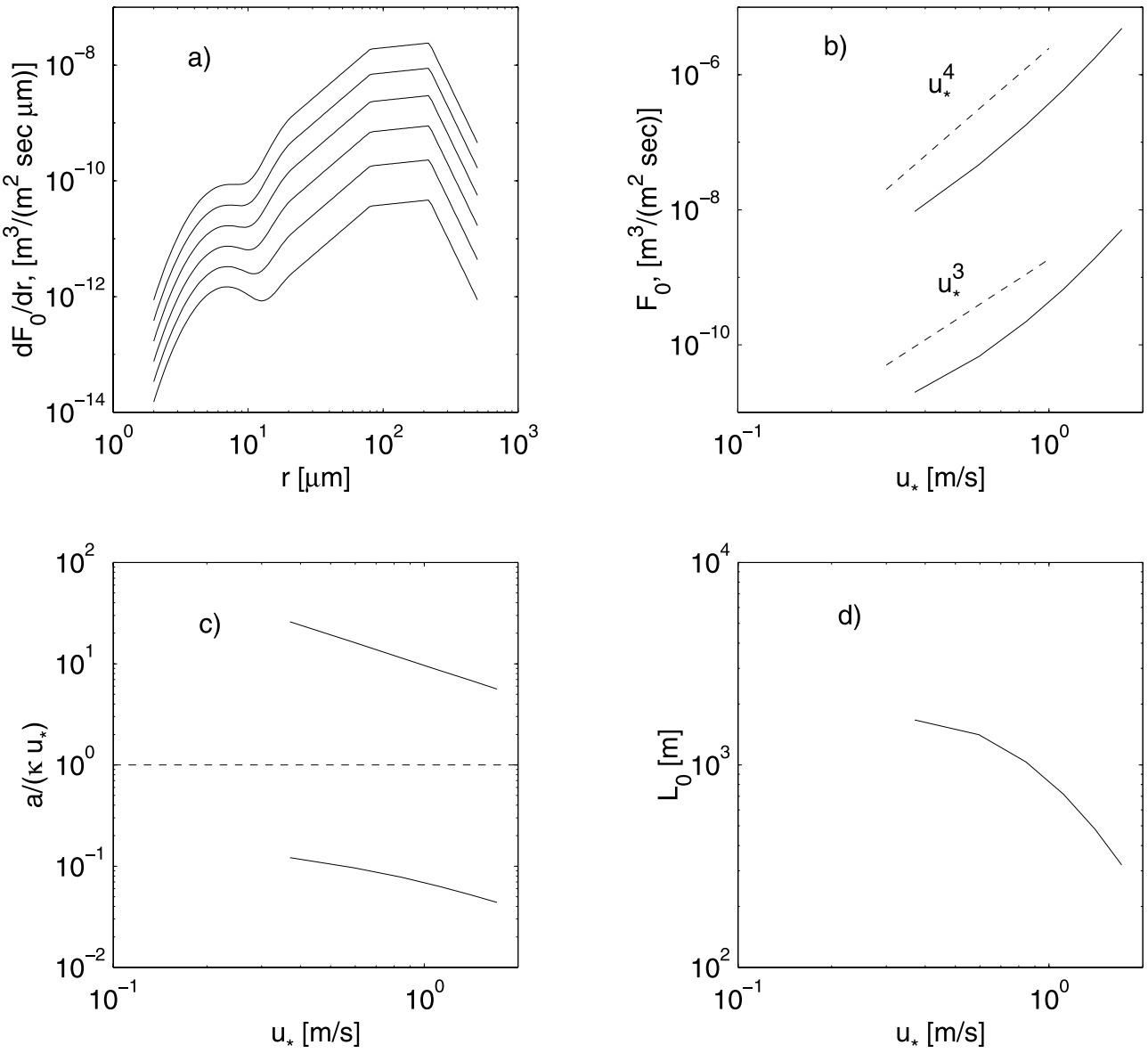

Figure 2. (a) Spray generation function (SGF) proposed by *Andreas* [1998] at wind speeds from 10 m/s to 35 m/s (over 5 m/s), corresponding curves are from the bottom to the top. (b) Wind dependence of the integral SGF for the bubble droplets ($r < 20$ μm; lower solid line) and spume droplets ($r > 20$ μm; upper solid lines) which calculated through (37) with spectral SGF shown in Figure 2a. (c) Dimensionless fall velocity $\omega = a/(\kappa u_*)$ versus u_* for the bubble (low solid line) and spume (upper solid line) droplets with radius defined by (36). (d) Stratification length scale (29) versus friction velocity.

in Figure 2b indicated that the effect of "real" spray on MABL is negligible, and thus not shown. For instance, it was found that even at the highest wind speed $u_{10} = 50$ m/s the sea spray reduce C_{dh} on 0.1% only.

[28] As discussed by *Andreas* [1998], empirical estimates of SGF are quite controversial and demonstrate a large scatter in the magnitude. A question rises, could a possible uncertainty in the SGF magnitude enlarge the impact of drops? To find an answer, we made the calculations with *Andreas*'s [1998] SGF enhanced in 10-, 10^2- and 10^3-times in the magnitude. In the two first cases, no remarkable effect was revealed. When SGF is enhanced in 10^3-times, a pronounced effect of bubble droplets on MABL has appeared (though the impact of spume droplets was still weak). Figure 3 shows the drag coefficient (38) for the reference level and the drag coefficient $C_{d10} = u_*^2/u_{10}^2$ for the "standard" 10 m-level. When the SGF is enhanced in 3-orders, the impact of bubble droplets on C_{dh} becomes strong. At that wind speeds when $L_{s0} \gg 10$ m, the drag coefficient C_{d10} coincides with the reference (no droplets) one. When L_{s0} approaches 10 m, the drag coefficient C_{d10} rapidly drops.

[29] Figure 4 shows the wind velocity and the bubble droplets concentration profiles at $u_h = 80$ m/s. Effect of the droplets lead to significant deviation of the wind profile from the reference one, and results in a deceleration of the near surface wind (similar to the thermal stably stratified atmospheric boundary layer). Dash-dotted lines show the

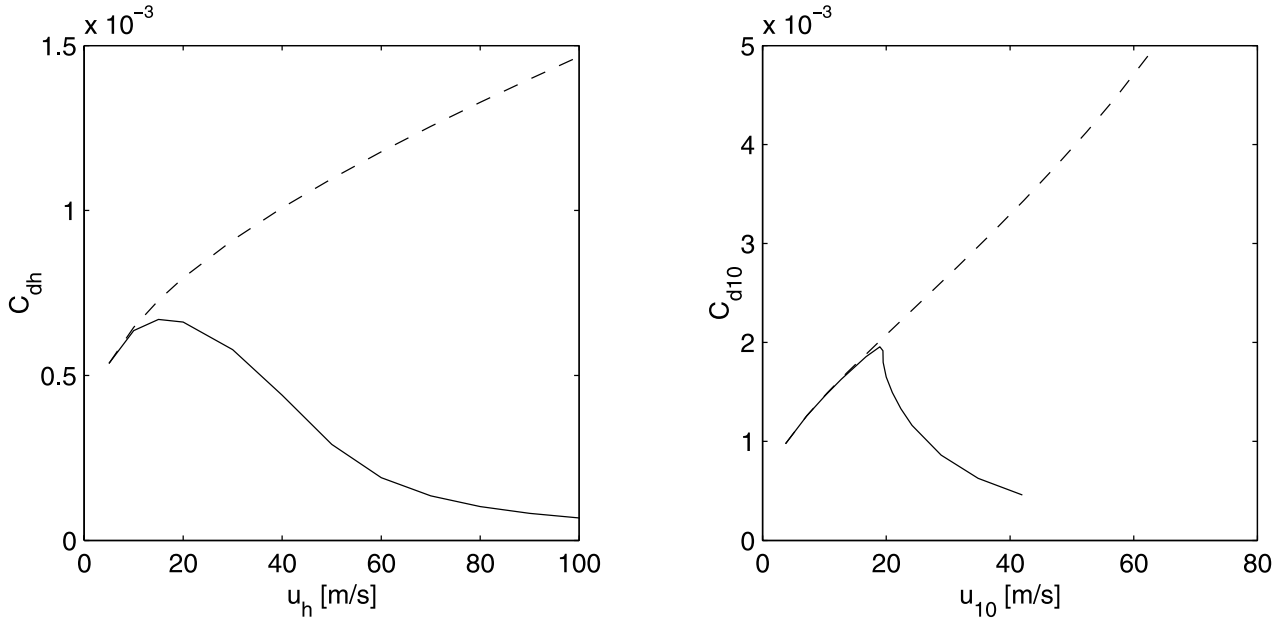

Figure 3. Drag coefficient for the reference level $h_r = 10^3$m versus reference wind speed u_h. (right) 10-m drag coefficient C_{d10} versus wind speed u_{10}.

asymptotic solutions (26) (at small z) and (35) (at large z), which fit well $u(z)$ at the height of their validity. The right plot in Figure 4 shows the vertical profile of the droplets concentration and asymptotic solutions (27) and (32), which again well fit $s(z)$ at small and large z correspondingly.

[30] To resume this section, we note the following:

[31] 1. The model adopting the real estimate of the SGF (as proposed by *Andreas* [1998]) and based on an assumption that the droplets (both bubble and spume) are ejected upward from the sea surface, cannot predict any significant effect of sea spray of the airflow dynamics.

[32] 2. The only possibility to achieve an effect is to enhance the SGF magnitude in 10^3-times. Such enhancement very likely exceeds a range of uncertainty in empirical estimates of the SGF. However, even at such strong enhancement, contribution of the spume drops to the effect is negligible in comparison with the bubble one.

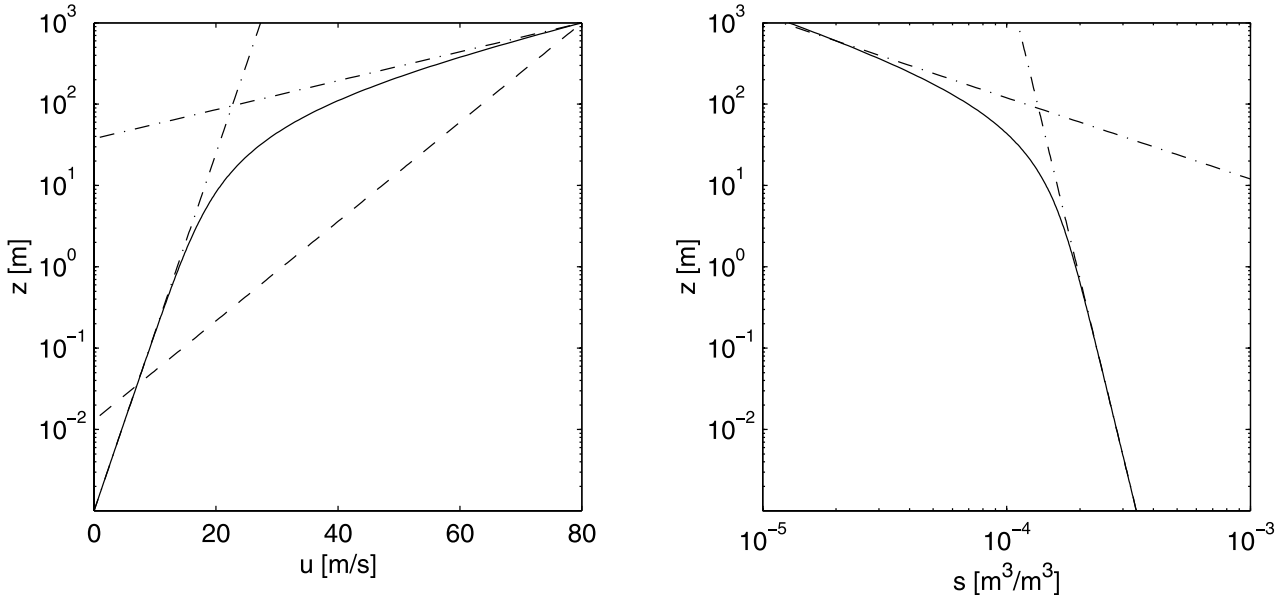

Figure 4. Profiles of wind velocity (left) and bubble droplets concentration (right) at reference wind speed $u_h = 80$ m/s. Solid lines are full solution of equations (25) and (24). Dash line in left plot shows the wind velocity profile when effect of droplets is "switched off". Dash-dot lines are the asymptotic solutions: (26) and (27) at small z, and (35) and (32) at large z.

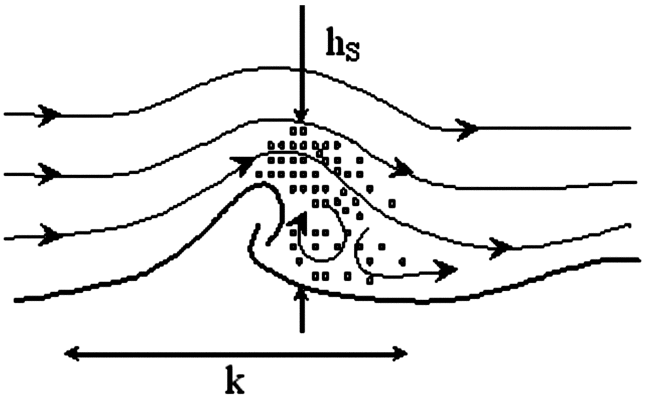

Figure 5. Sketch illustrating kinematics of the airflow (streamlines with arrows) over a breaking wave and spume drops (shown by dots) generation.

[33] Does it mean that the effect of sea spray is really weak, or that is a shortcoming of the considered above model?

4. Effect of Spray: Wind Tearing of Breaking Crests

[34] Assumption that sea drops are ejected upward at the surface is reasonable for the bubble droplets, and certainly is not applicable for the spume one. Spume droplets result from a mechanical tearing of breaking crests, and they are rather ejected ''horizontally'' into the airflow at some height, and then blown away by the wind. Since spume drops are relatively heavy, $\omega > 1$, they are finally falling back to the surface. As mentioned, the magnitude of the SGF for spume drops is conventionally established, but the question to what height this SGF should be applied, is still open. Nevertheless, since spume drops are created near the wave crests, one may suggest that some scaling with the wave amplitude is inevitable.

[35] The spume drops production by the wind tearing of wave crests was recently studied by *Anguelova et al.* [1999] in laboratory conditions. They found that the rate of spume drops production merges effectively when normalized on the number of wave breaking events. They concluded that the wave breaking occurrence is the dominant factor of the spume drops production.

4.1. Volume Source of Spume Droplets

[36] Spume drops are ejected into the airflow at the altitude of breaking waves crests. Though these waves can be relatively short, spume drops (in the mean) appear in the airflow well above the aerodynamic roughness height z_0. Therefore, to take into account this fact, we introduce a volume source I_s in (3) (or s_* in (13)) which describes mean rate (i.e. averaged over many periods of the spectral peak waves) of spume drops production per unit volume by all breaking wind waves (including breaking crests of dominant waves).

[37] In order to derive this source we start with an assumption of a narrow band surface waves with the mean wavenumber k. Sporadically, crests of these waves break and lose the energy coming from the wind. At the same time, wind tears the breaking crests and generates spume droplets. Kinematics of the airflow over breaking waves is quite complicated, and the most extensive study of this phenomenon was performed in laboratory conditions by *Reul et al.* [1999] with use of DPIV technics. The main observed features are separation of the airflow from steep breaking crest and its re-attachment on the front slope of the following wave, and re-circulating well-organized vortex in the separation zone. Once torn off from the crest, the drops carry away by the airflow along its streamlines, and fill both the separated zone and the area ahead the breaking crest. Scheme of the airflow kinematics and spume drops generation is shown in Figure 5.

[38] Let us suggest that during the time interval T a large enough number N of wave breaking events has occurred on the sea surface area A. The mean life span of breaking waves is t_b, and the length of an individual breaking crest is l_b^i. The volume v_s^i of droplets torn off by wind from an individual breaking crest during its life span is

$$v_s^i = F_s t_b h_s l_b^i \tag{39}$$

where F_s is the flux of spume droplets, and h_s is a height of the layer where spume drops are distributed (see Figure 5); we assume that $h_s \propto k^{-1}$, i.e., the longer is the wave the higher level of the drops ejection. Then the total volume of spume drops pulverized into the airflow volume $v_a = h_s A$ from all breaking waves is

$$v_s = \sum^N v_s^i = F_s t_b h_s \sum^N l_b^i \tag{40}$$

and the volume source of droplets (the rate of droplets production in a unit volume of the air) $dV_s = v_s/(v_a \cdot T)$ is

$$dV_s = \frac{F_s t_b h_s \sum^N l_b^i}{h_s A T} = F_s \frac{\sum^{N_A} l_b^j}{A} \tag{41}$$

To derive the last equation (41) we took into account that the number N of breaking events appearing on the area A during the time interval T relates to the number N_A of breaking events on the same area at any instant moment as: $N = N_A T/t_b$, and thus

$$\sum^N l_b^i = (T/t_b) \sum^{N_A} l_b^j \tag{42}$$

[39] As assumed, the length of wave breaking fronts per unit surface area $\sum^{NA} l_b^j/A$ is related to the waves of a narrow band, from $\mathbf{k}$ to $\mathbf{k} + d\mathbf{k}$. This quantity is the spectral surface density of wave breaking fronts originally introduced by *Phillips* [1985]:

$$\sum^{N_A} l_b^j/A = \Lambda(\mathbf{k}) d\mathbf{k} \tag{43}$$

Then equation (41) takes the form

$$dV_s(z) = F_s H(\epsilon - kz)\Lambda(\mathbf{k})d\mathbf{k} \tag{44}$$

where ϵ is a constant relating h_s to k, $h_s = \epsilon/k$, and $H(x)$ is the Heaviside step function truncated action of the volume source at $z > \epsilon/k$. The total volume source of spume drops to be found by integration of (44) over all scales of breaking waves, and reads:

$$V_s(z) = F_s \int_{\mathbf{k}} H(\epsilon - kz)\Lambda(\mathbf{k})d\mathbf{k} = F_s \int_{|\mathbf{k}|<\epsilon/z} \Lambda(\mathbf{k})d\mathbf{k} \tag{45}$$

Quantity $\Lambda(\mathbf{k})$ also defines the rate of energy dissipation in breaking waves [*Phillips*, 1985]

$$dD \propto g^{-1}c^5\Lambda(\mathbf{k})d\mathbf{k} \tag{46}$$

where c is wave phase velocity. Since dD is proportional to the wind energy input

$$dI_w = g\varpi\beta k^{-4}B(\mathbf{k})d\mathbf{k} \tag{47}$$

(ϖ is wave frequency) the wave breaking statistics $\Lambda(\mathbf{k})$ can be expressed in terms of the wind wave growth rate β and the saturation spectrum $B(\mathbf{k})$ as

$$\Lambda(\mathbf{k}) \propto k^{-1}\beta B(\mathbf{k}) \tag{48}$$

The growth rate parameter β is $\beta \propto (u_*/c)^2$ [e.g., *Plant*, 1982]. It is normally accepted that the saturation spectrum is proportional to u_*/c in some power: e.g., $B \propto (u_*/c)$ [*Toba*, 1973; *Donelan et al.*, 1985], $B \propto (u_*/c)^{0.2\pm0.2}$ [*Banner et al.*, 1989].

[40] *Melville and Matusov* [2002] provided a description of the wave breaking distribution at the ocean surface. They found that the length of wave breaking fronts is proportional to the cube of the wind speed. In order to be consistent with these observations, we estimate $\Lambda(\mathbf{k})$ via (48) with the saturation spectrum $B(k) \propto u_*/c$:

$$\Lambda(\mathbf{k}) \propto k^{-1}\left(u_*/c\right)^3 \tag{49}$$

This equation is valid at $k < k_b$, where k_b is the wavenumber of shortest breaking waves generating white caps and thus spume drops. An estimate of k_b is $k_b \approx 10$ rad/m. Then equation (45) with (49) can be rewritten as

$$V_s(z) \propto F_s k_b\left(u_*/c_b\right)^3 f_V(z/z_b) \tag{50}$$

where $c_b = (g/k_b)^{1/2}$ is phase velocity of shortest breaking waves, $z_b = \epsilon/k_b$, and f_V is the volume source profile function equal to $f_V = (z_b/z)^{5/2}$ at $z/z_b > 1$ and $f_V = 1$ at $z \le z_b$. From the top, $V(z)$ is bounded by $z = \epsilon/k_p$. However, contribution of the breaking waves rapidly (as $\propto k^{5/2}$) reduces with decreasing wavenumber, and we shall ignore a small drop of $V(z)$ at $z = \epsilon/k_p$. The integral volume source $I_s(z)$ of spume drops in (3) is defined as

$$I_s(z) = \int_z^\infty V_s(z)dz \propto 2/3\epsilon F_s(u_*/c_b)^3 f_I(z/z_b) \tag{51}$$

with $f_I = (z_b/z)^{3/2}$ at $z/z_b > 1$ and $f_I = 1 + 3/2(1 - z/z_b)$ at $z/z_b \le 1$. Sources $V_s(z)$ and $I_s(z)$) are rapidly decreasing functions of the height. This is a consequence of that the shorter are the waves the larger is their contribution to the total length of breaking crests, and thus to spume drops production.

[41] To define the rate of spume drops generation from an individual breaking crest (term F_s in (51) and (50)), we shall follow the thermodynamic approach proposed by *Andreas et al.* [1995]. The energy required to form a single droplet is:

$$\Delta e = 4/3\pi\gamma r^2 \tag{52}$$

where γ is the surface tension. If the spume droplets are produced continually by the wind tearing with the rate N_s (the number of droplets produced per unit time from unit area), then

$$4/3\pi\gamma r^2 N_s \propto u_s^3 \tag{53}$$

where u_s is the scale of the wind speed. Since $F_s = 4/3\pi r^3 N_s$, we have the following equation for F_s:

$$F_s = c_* \frac{r u_s^3}{\gamma} \tag{54}$$

where c_* is a constant to be defined after a comparison with measurements. Then the volume (50) and the integral volume source (51) of spume droplets take the form

$$V_s(z) = c_* \frac{r u_s^3}{\gamma} \cdot \left(\frac{u_*}{c_b}\right)^3 k_b f_V(z/z_b) \tag{55}$$

$$I_s(z) = \frac{2}{3}\epsilon c_* \frac{r u_s^3}{\gamma} \cdot \left(\frac{u_*}{c_b}\right)^3 f_I(z/z_b) \tag{56}$$

These relations predict a very strong wind dependence of the spume drops production, with the wind exponent near 6. As mentioned above, both enhanced wave breaking and acceleration of the airflow produce an auspicious conditions for spume drops generation on the crests of dominant waves. To take into account this fact we assume that the wind scale u_s in (54) is the wind speed at height of the sea surface standard deviation, i.e. $u_s = u(\sigma_\zeta)$.

[42] Note the following. As it follows from (49), length of breaking fronts is an increasing function of both k and u_*. Therefore one may anticipate that at very high winds exceeding some "threshold" wind speed, $\Lambda(\mathbf{k})$ will be saturated at

$$\Lambda(k) \propto k^{-1} \tag{57}$$

We may assume that saturation of $\Lambda(\mathbf{k})$ starts at shortest breaking waves and in the course of the wind increasing will spread towards the larger breaking scale. In this case volume source $V(z)$ (45) tends to

$$V_s(z) \propto \frac{r u_s^3}{\gamma z} \tag{58}$$

In the regime of wave breaking saturation, the volume source attenuates with the height slower (z^{-1} instead of $z^{-5/2}$ in (55)) and rate of spume drops production is cubic in wind speed, i.e., is twice less than in (55). Presumably, this regime may be realized at the highest hurricane winds when conception of the air-sea interface becomes relative as the sea surface is totally covered by the foam and near surface concentration of the sea drops is very large. Analysis of such conditions is out of the scope of the present study.

4.2. Wind and Spume Drops Profiles and Resistance Law

[43] As shown in section 3, the "real" bubble droplets cannot affect the MABL dynamics unless the rate of their production is enhanced in 10^3-times. Such strong enhancement exceeds the limits of uncertainty in the empirical SGF, and further the effect of bubble droplets is ignored.

[44] Solution of equation (13) with the volume source (55) and the boundary condition $\partial s/\partial z = 0$ at $z = z_0$ reads

$$s(z) = s_*(z) - \int_{z_0}^{z} \exp[-\omega[\hat{u}(z) - \hat{u}(z')]] v_*(z') dz' \tag{59}$$

where $\hat{u}(z) = (\kappa/u_*)u(z)$ is normalized velocity, $s_*(z) = I_s(z)/a$ is the droplets concentration produced by the integral volume source, and $v_* = V_s(z)/a$. Second term in the r.h.s. of (59) describes contribution of turbulent mixing on the vertical distribution of spume drops. Equations (59) and (25) with (21) can be easy solved numerically for an arbitrary spectral volume source, describing rate of production of spume drops of different radius.

[45] However, here we are considering a "monochromatic" spume drops with the size corresponding to the mean observed radius, $r_m = 180$ μm. We remind that for the such drops dimensionless fall velocity ω is rather large (see Figure 1c). In this case, the integral in the r.h.s. of (59) can be evaluated approximately, and equation (59) accurate to the order $1/\omega$ reads.

$$s(z) \simeq s_*(z) + \omega^{-1} z v_*(z) \tag{60}$$

i.e., concentration of the spume drops is mainly resulted from the balance of their tearing off from breaking crests and falling down due to gravitation (so-called "rain" of drops). The length scale (21) now is

$$\frac{1}{L_s(z)} = \kappa^2 \sigma z v_*(z) \frac{g}{u_*^2} \tag{61}$$

With use of (61) and (55) the wind profile (25) is rewritten as

$$u(z) = \frac{u_*}{\kappa}\left[\ln\left(\frac{z}{z_0}\right) + d\omega^{-1}\frac{F_s}{c_b} f_u(z/z_b)\right] \tag{62}$$

where $d = \kappa\epsilon^2\sigma/(2Ko_{cr})$ is a constant adopting other constants, and f_u is a wind velocity profile correction function, which is equal to $f_u = (z/z_b)^2$ at $z/z_b < 1$ and $f_u = 5 - 4(z/z_b)^{-1/2}$ at $z/z_b \geq 1$. Notice that according to this equation, effect of spume drops on wind profile decreases with increase of the drops size, and at $\omega = \infty$ effect is disappeared. The physical meaning is that very large drops (torn off from breaking crests) are falling too fast to affect the turbulence while they are airborne.

[46] At $z/z_b \gg 1$ the wind velocity profile reads

$$u(z) = \frac{u_*}{\kappa}\left[\ln\left(\frac{z}{z_0}\right) + 5\omega^{-1} d\frac{F_s}{c_b}\right] \tag{63}$$

$$= \frac{u_*}{\kappa}\ln\left(\frac{z}{Z_0}\right) \tag{64}$$

where Z_0 is the effective roughness scale defined as

$$Z_0 = z_0 \cdot e^{-5\omega^{-1} dF_s/c_b} \tag{65}$$

with z_0 corresponding to the Charnock relation (23). The rate of the spume drops production from a breaking crest F_s is cubic in wind speed, thus Z_0 rapidly decreases at strong winds. We emphasize again, that since $\omega \propto r^2$ and $F_s \propto r$ effect of drops on the effective aerodynamic roughness become weaker at increasing drops size.

[47] The wind scale u_s defining F_s by (54) was determined as the wind speed at the height the sea surface standard deviation, $z = \sigma_\zeta$, thus with use of (62) the scale u_s is

$$u_s = \frac{u_*}{\kappa}\left[\ln\left(\frac{\sigma_\zeta}{z_0}\right) + 5\omega^{-1} d\frac{F_s}{c_b}\right] = \frac{u_*}{\kappa}\ln\left(\frac{\sigma_\zeta}{Z_0}\right) \tag{66}$$

[48] In order to determine the tuning constant c_* in (54), we shall use the data for the rate of production of spume drops surface area F_A (its dimension $[F_A] = \mathrm{m}^2/\mathrm{m}^2/\mathrm{sec}$) which were analyzed in [*Andreas*, 1998], and shown here in Figure 6. Quantity F_A relates to the integral volume source $I_s(z)$ as: $F_A(z) = 3I_s(z)/r$. The shaded area in Figure 6 is the model values of F_A with the tuning constant $c_* = 5 \cdot 10^{-9}$ and $k_b = 20$ rad/m, $\varepsilon = 2$. The upper and lower bounds of this area correspond to $F_A(z)$ at $z = 0.2$ m and $z = \sigma_\zeta$ (for mature seas) respectively. In this range of z the data shown in Figure 6 were presumably collected. Empirical relations are quite different in magnitude of F_A and its wind dependence. However, the model values are inside the area covered by the empirical curves, and this value of c_* is further used in the model calculations. Notice, that the only upper bound of the shaded area in Figure 6 indicates wind exponent of F_A; a different slope of the lower bound is caused by dependence of σ_ζ on wind speed. Notice also that the model wind exponent in Figure 6 is rather "5" than "6" as expected from (56). This results from that the wind scale u_s is not simply proportional to u_*, but varies so as $u_s^3 \propto u_*^2$.

[49] To see how the sea drops affect the whole MABL, we adopt a simplified model of the planetary boundary layer model proposed by *Brown* [1982]. Some details of this model are given in Appendix A. The wind profile in the

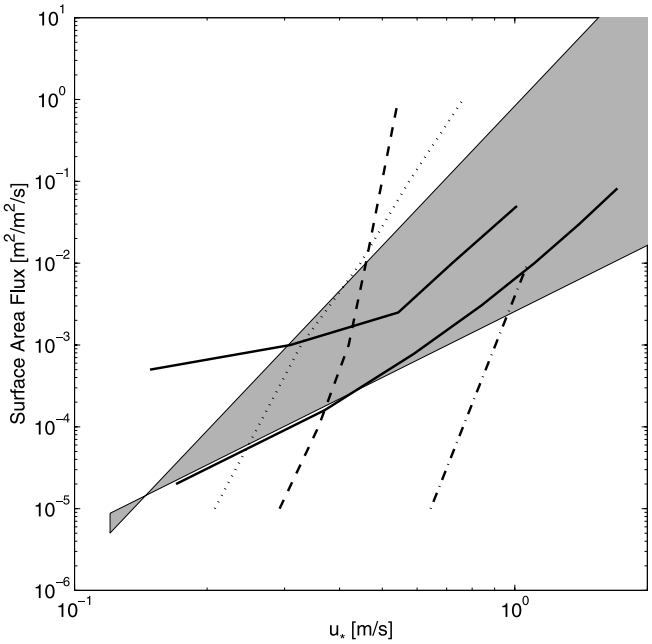

Figure 6. Rate of production of spume droplets surface area F_A versus friction velocity. Shaded area is the model values $F_A = 3I_s(z)/r$ with $I_s(z)$ defined by (56) for z in the range from $z = 0.2$ m (upper bound) to $z = \sigma_\zeta$ (lower bound), σ_ζ is the standard deviation of the sea surface. Empirical data are shown by: dash-dot line [*Wu*, 1993], dash line [*Monahan*, 1986], dotted line [*Iida et al.*, 1992], upper solid line [*Andreas*, 1992], lower thin solid line [*Andreas*, 1998], modified [*Smith et al.*, 1993].

Ekman part of the planetary MABL (at $z > h$, where h is defined by (A3)) is given by

$$\mathbf{u}(z) - \mathbf{G} = -\frac{(1-i)}{2\varepsilon}\frac{\mathbf{u}_*}{\kappa}\exp\left[-(1+i)\frac{z-h}{H}\right] \qquad (67)$$

where **G** is the geostrophic wind velocity; the bold symbols denote complex variables where the argument corresponds to a vector direction (the geostrophic velocity or the wind stress). This profile provides continuity of the momentum flux at the lower boundary of the Ekman boundary layer, $z = h$. Patching wind profiles (64) and (67) at $z = h$ results in the resistance law for the planetary boundary layer (see also (A5))

$$\frac{\mathbf{u}_*}{\mathbf{G}} = \kappa\left[\ln\left(2\varepsilon^2\frac{\kappa u_*}{fZ_0}\right) + \frac{(1-i)}{2\varepsilon}\right]^{-1} \qquad (68)$$

Thus the geostrophic wind speed is the only external parameters of the problem. Solution of the equation for the resistance law (68) with the effective roughness scale (65) gives the friction velocity u_* in the MABL, that in turn defines the full description of the MABL, - its wind profiles (equations (62) and (67)) and the spume droplets distribution (60).

5. Model Results and Comparison With Observations

[50] The resistance law (68) with (65) is solved by iterations. Figure 7 shows the geostrophic drag coefficient $C_D = (u_*/G)^2$ and the deviation φ_* of the surface wind stress from the direction of the geostrophic wind velocity. The model calculations with and without (reference run)

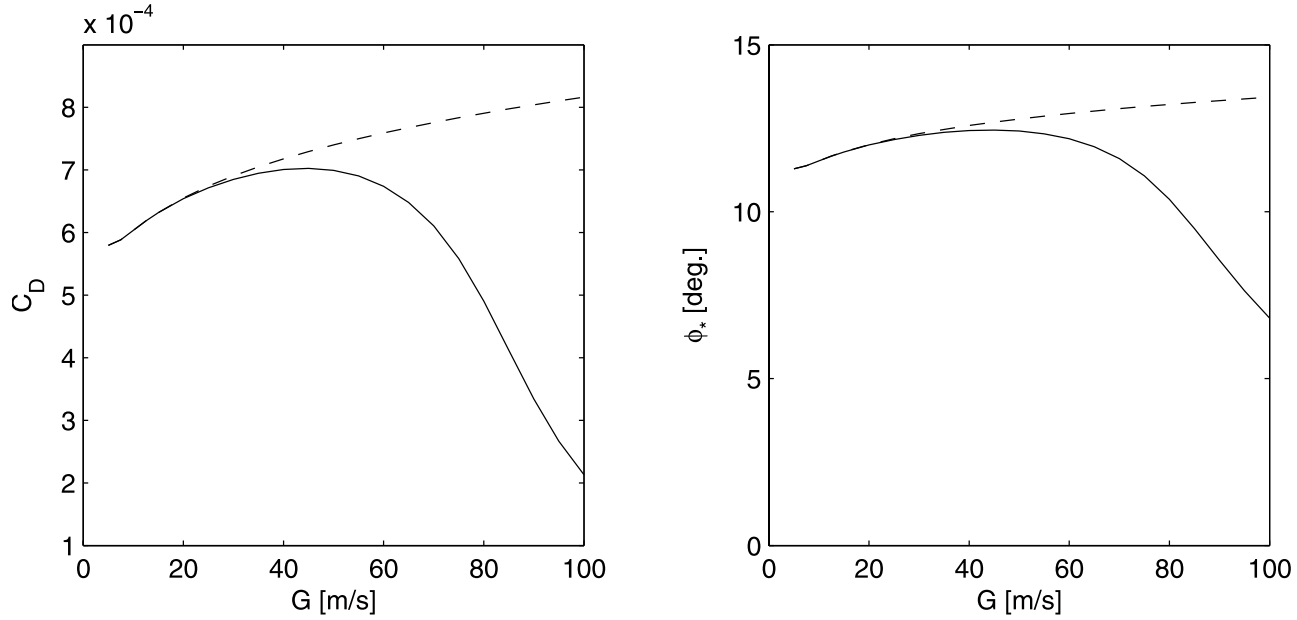

Figure 7. Geostrophic drag coefficient $C_D = (u_*/G)^2$ (left), and angle between surface wind stress and geostrophic wind velocity (right) as a function of G calculated on the resistance law (68). Dash lines are the reference (no spray effect) calculations. Solid line correspond to the calculations with the effective roughness scale (65) which accounts for the effect of sea drops.

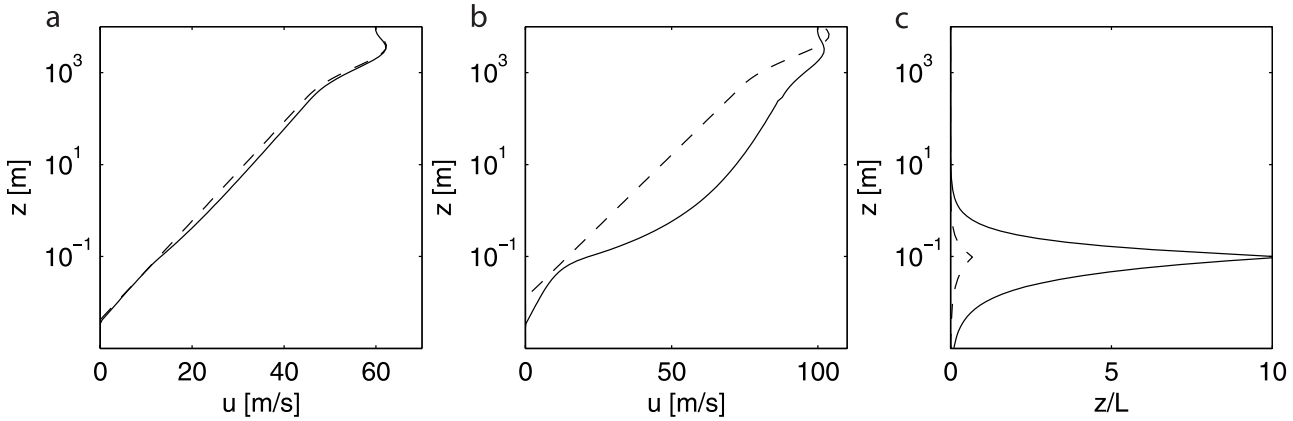

Figure 8. Wind speed profile in the MABL at (a) G = 60 m/s and (b) G = 100 m/s. Dash lines in Figures 8a and 8b are reference (no spray effect) calculations, and solid lines are calculations on full model. (c) Profiles of the stratification parameter z/L at G = 60 m/s (dash line) and G = 100 m/s (solid line).

accounting for the effect of the spume droplets are plotted. Departure of the geostrophic drag coefficient from the reference one starts at G around 30 m/s. With the increasing wind speed a strong generation of spume droplets results in a rapid drop of the surface drag. Suppression of the surface drag is accompanied with a rotation of the wind surface stress towards the geostrophic wind direction.

[51] Figures 8a and 8b show the wind velocity profiles at G = 60 m/s and 100 m/s, and Figure 8c shows vertical distribution of the stratification parameters $z/L(z)$ (with L defined by (61)) at these wind speeds. Maximum of $z/L(z)$ is located approximately at the altitude of the shortest breaking wave crests, and z/L rapidly attenuates with increasing height. According to (22) wind velocity shear directly depends on z/L. At large values of z/L wind velocity shear deviates from the reference one that results in an acceleration of the airflow. Thus suppression of turbulent mixing (and the surface drag) and acceleration of the airflow is the coupled effect of spume drops on MABL dynamics. Notice an apparent reduction of the planetary MABL depth (which is proportional to the height of the local maximum in the wind speed profile) in comparison with the reference one.

[52] A standard representation of the model results in terms of the drag coefficient at 10-meter height, C_{d10}, is shown in Figure 9. The drag coefficient starts to deviate from the reference one at wind speeds above 20 m/s, and at $u_{10} > 30$ m/s C_{d10} rapidly drops to very low values. Dependence of the friction velocity on u_{10} is not

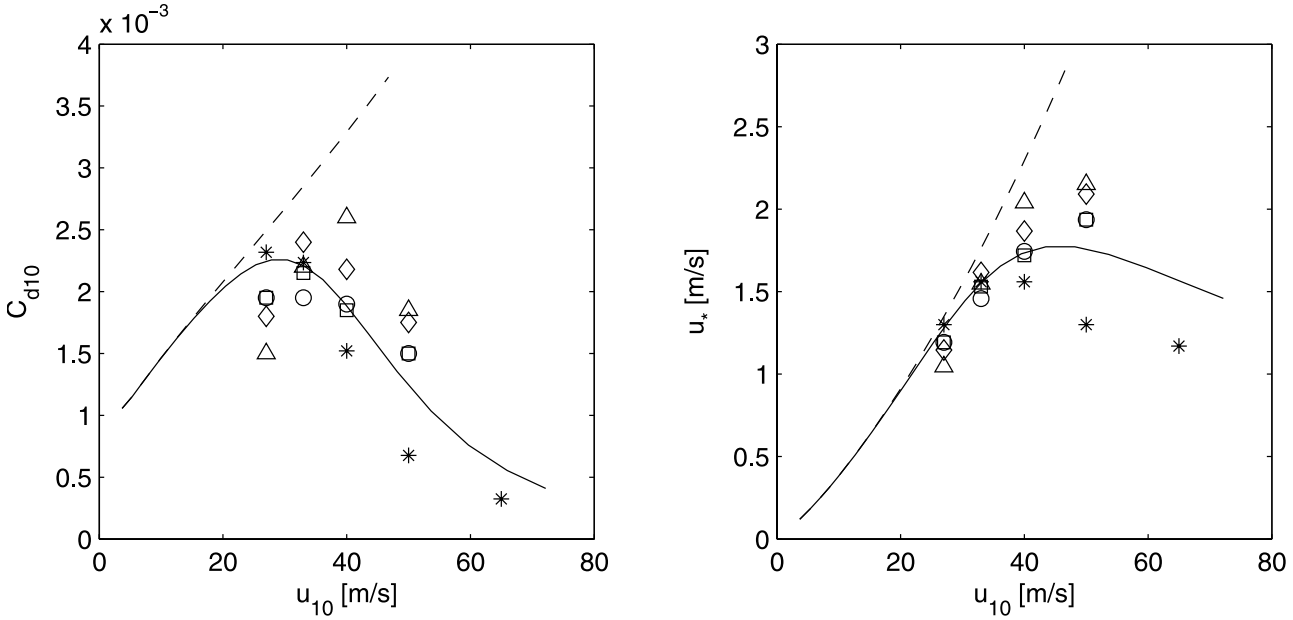

Figure 9. Drag coefficient C_{d10} (left) and friction velocity u_* (right) versus wind speed at 10 m height. Dash lines are reference calculations (no effect of sea drops) for the Charnock roughness scale (23). Solid lines are model calculations corresponding to the roughness scale (65) which accounts for the effect of sea drops. Open symbols are data taken from *Powell et al.* [2003, Figures 3a and 7c]. Stars are estimates of C_{d10} and u_* listed in Table 1.

Table 1. Estimates of u_* Via Wind Profiles

G, m/s	u_{10}, m/s	z_{max}, m	u_*, m/s	$C_{d10} \cdot 10^3$
34–39	27	500	1.30	2.32
40–49	33	600	1.56	2.23
50–09	40	600	1.56	1.52
60–69	50	500	1.30	0.68
70–85	65	450	1.17	0.32

monotonic,- at $u_{10} < 40$ m/s u_* is a growing function of u_{10}, and then at stronger winds u_* (due to the suppression of the surface drag) is leveling off and tends to decrease.

[53] Note that at $u_{10} > 45$ m/s the model surface concentration of drops attains relatively large values and parameter σs_0 becomes of order 1. As mentioned, validity of the governing equation requires parameter $\sigma\ s_0$ be small. Therefore some heed of interpretation of model results at highest wind speeds is needed.

[54] Significant reduction of the surface drag in real conditions at wind speeds over 40 m/s was first reported by *Powell et al.* [2003]. Open symbols in Figure 9 are the data taken from *Powell et al.* [2003, Figures 3a and 3c]. As was noted, at $u_{10} < 30$ m/s their data on C_{d10} are consistent with numerous investigations. However, at winds approaching the hurricane force (30 m/s) C_{d10} levels off and then falls down at higher winds. In overall, the model calculations agree with the data, though the model u_* levels off at smaller wind speed than it could be expected from the data.

[55] To extract more information from this unique data (especially for the case of highest wind speeds 70–85 m/s where *Powell et al.* [2003] were failed to assess z_0 through fitting by the least-square line the wind profile) we make an attempt to assess u_* through the vertical scale of the MABL. According to the similarity theory for the planetary boundary layer [*Kazanski and Monin*, 1961], the wind velocity profiles in the Ekman part of the MABL are universal functions of the dimensionless height zf/u_*. If we assume that the similarity theory may be applied for the tropical cyclones, then a remarkable feature in the wind profiles may be used to assess u_*. As an apparent feature we choose height z_{max} of the local maximum in the wind speed profiles, which is well pronounced in Figure 2 of *Powell et al.* [2003]. The eye-ball estimate of z_{max} as well as corresponding values of u_{10} are listed in Table 1. According to the similarity theory, the dimensionless height z_{max} to be a constant, i.e.,

$$z_{max} f / u_* = const \tag{69}$$

We have defined the constant in (69) so as to have an "expected" value of $u_* = 1.3$ m/s at the lowest wind speed $u_{10} = 27$ m/s. Then this constant was further used to assess u_* for the other cases. The estimate of u_* and corresponding values of $C_{d10} = (u_*/u_{10})^2$ are also listed in Table 1 and plotted in Figure 9. These estimates demonstrate much more pronounced suppression of the surface drag at strong winds. Reduction of the drag is so strong that it leads to decrease of the friction velocity at $u_{10} > 40$ m/s.

[56] Saturation of the C-band backscatter from the sea surface at high wind speeds (>25 m/s) was observed by *Donnely et al.* [1999]. It is normally accepted that a spectrum of the surface roughness scattering radiowave depends on the air friction velocity. If we adopt this assumption, then the saturation of the backscatter may be interpreted as a saturation of the surface stress at wind speeds above 25 m/s, and thus decrease of the sea surface drag coefficient as predicted by the present model.

[57] All the equation discussed above are written in the wave following coordinate system, and a question may arise is how does profile of any quantity in this coordinate system relate to the profile in the regular fixed Cartesian coordinate system. As mentioned in section 2, any mean quantity $Y(z)$ in wave-following coordinate system can be transformed to the mean quantity in the fixed Cartesian coordinate system as $Y(x_3) = \overline{Y(z(x_3))}$, where the wave-following z and Cartesian x_3 coordinates are linked by (8). Figure 10 shows

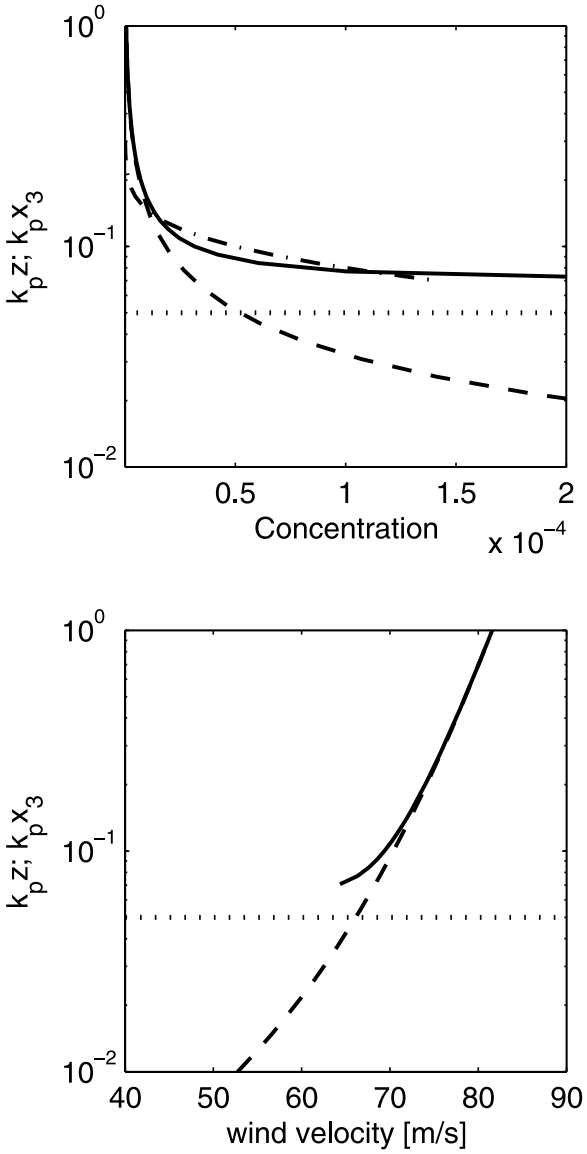

Figure 10. Comparison of sea drops concentration (top) and wind velocity (bottom) profiles in the wave-following (dash lines) and fixed (solid lines) coordinate system at geostrophic wind speed 100 m/s. Dotted lines indicate standard deviation of the model sea surface. Dash-dotted lines in the top plot is empirical profile (70).

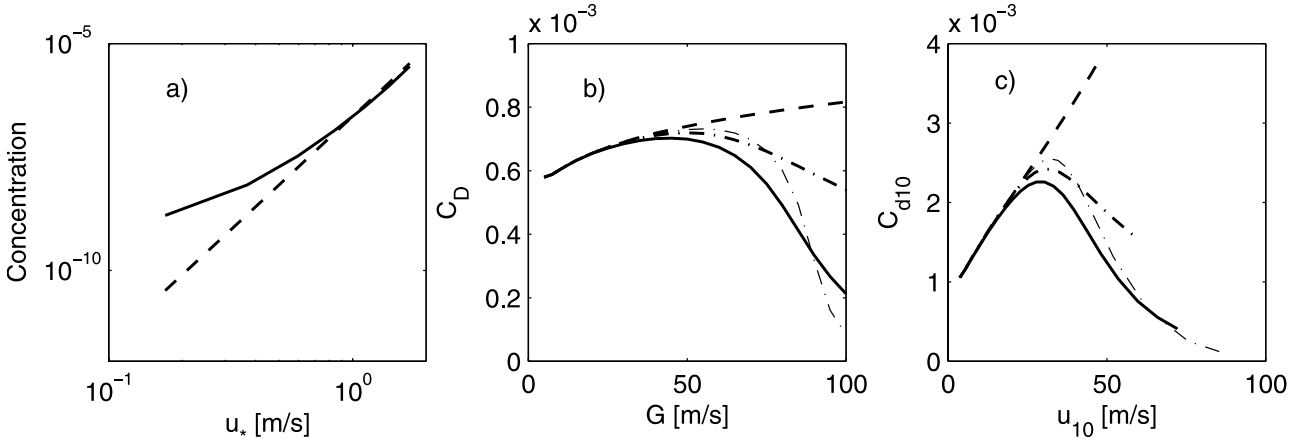

Figure 11. (a) Wind dependence of the surface concentration of droplets s_0 (solid line) defined through SGF shown in Figure 2a as: $s_0 = \int a^{-1}(dF_0/dr)dr$. Dash line is $s_0 = 2.5 \cdot 10^{-7}\, u_*^5$ which fits empirical curve at high wind speeds. (b) and (c) Geostrophic drag coefficient (C_D) and 10-meter drag coefficient (C_{d10}). Solid lines are the model calculations with roughness scale (65) (the same as in Figures 6 and 8). Dash lines are reference calculations (no effect of sea drops). Dash-dot lines are model calculations with the effective roughness scale (75) and "empirical" concentration (76) (thick dash-dot lines) and (77) (thin dash-dot lines).

fragments of spume drops and wind velocity profiles at G = 100 m/s in both coordinate system. Unlike wave-following coordinate system, profiles of s and u in the fixed coordinate system have a meaning above the wave crests only. Dotted lines in this figure indicate standard deviation of the model wavy surface. Concentration of spume drops is strongly stratified, therefore profiles of s in the wave-following and fixed coordinate systems are very different. In the fixed coordinate system profile of s is sharper, and it is in qualitative agreement with empirical profile shown by dash-dotted line (see equation (70) below). Wind velocity profile in the wave-following coordinate system is relatively "smooth", thus the difference between profiles is rather small.

6. Discussion

[58] As shown in section 3.2, model calculations based on assumption that spume drops are ejected upward at the surface can predict no significant effect unless "real" SGF is enhanced in 10^3-times. On the other hand, the model based on assumption that spume drops are ejected at altitudes of the breaking crests, predicts quite strong effect. Therefore one can conclude that vertical spreading of spray generation plays a crucial role.

[59] It is worthy to check what model does predict if vertical profile of spume drops concentration is imposed empirically. Normally, the vertical profile of droplets concentration is scaled with the significant wave amplitude A_s, as, e.g., in [*Andreas*, 2004]:

$$s(z) = s_0 \exp(-z/\delta) \tag{70}$$

where $\delta = c_\delta A_s$ is a vertical scale, $c_\delta = 0.3$, $A_s = 10^2 u_*^2/g$, and s_0 is surface concentration of drops. Surface concentration can be estimated through empirical SGF discussed in section 3.2 (and shown in Figure 2a) as $s_0 = \int a^{-1}(dF_0/dr)dr$. Wind dependence of s_0 is plotted in Figure 11a. At highest wind speeds, trend $s_0 \propto u_*^5$ can be easily observed and it is shown by dash line. Since we are focusing on the high wind conditions, we parameterize empirical wind dependence of s_0 as: $s_0 = 2.5 \cdot 10^{-7} u_*^5$.

[60] Adoption of empirical profile (70) excludes use of equations (21) and (20) (and correspondingly (22)) which are essentially based on the model drops conservation equation. Instead, we return to the Kolmogorov number defined through the gradient of sea drops concentration, equation (6). In this case relation of Ko to parameters of the boundary layer is:

$$Ko = z/L_{se}(1 - Ko/Ko_{cr})^2 \tag{71}$$

$$1/L_{se} = \kappa^2 \sigma z s_z(z) g/u_*^2 \tag{72}$$

where s_z is vertical gradient of drops concentration. These equations combined with (19) define the wind velocity shear (14). Notice, that substituting to (72) the model $s_z(z)$ we arrive again at the equations discussed in section 2.1. For the sake of simplicity, we assume that the empirical stratification parameter z/L_{se} is small enough. Then inverse mixing length function is approximately $1/\Phi \simeq 1 + Ko^{-1}{}_{cr} z/L_{se}$, and velocity shear (14) is then reduced to (22), and with use of (70) the wind velocity profile reads

$$u(z) = \frac{u_*}{\kappa}[\ln(z/z_0) + d_e s_0(1 - \exp(-z/\delta)(1 + z/\delta))] \tag{73}$$

where $d_e = 10^2 c_\delta \kappa^2 \sigma / Ko_{cr}$ is a constant (or a function of wave age if wind sea is not developed). At $z \gg \delta$ wind profile reads

$$u(z) = \frac{u_*}{\kappa} \ln(z/Z_0) \tag{74}$$

where Z_0 is the effective roughness scale defined as

$$Z_0 = z_0 e^{-d_e s_0} \tag{75}$$

with z_0 defined by the Charnok roughness scale (23). Since s_0 is strongly wind dependent, this equation predicts a fast decrease of the effective roughness scale, if surface concentration of drops is large enough.

[61] Model calculations with the original *Andreas* [1998] SGF gave a small effect on the surface drag (C_{d10} is reduced on 10% or less) and thus not shown. In order to simulate dynamics of the tropical cyclones, *Andreas and Emanuel* [2001] proposed to use a ''heuristic'' spray generation model, which is in 10-times amplified SGF shown in Figure 1b. In terms of the sea drops surface concentration a similar ''heuristic'' model is:

$$s_0 = c_s u_*^5 \tag{76}$$

with $c_s = 2.5 \cdot 10^{-6}$. As an alternative, we also consider the similar dependence, but scaled with wind speed at altitude of significant wave amplitude:

$$s_0 = C_s u_{A_s}^5 \tag{77}$$

where $u_{As} = u_*/\kappa \ln(A_s/Z_0)$ is wind speed at $z = A_s$, and C_s is a constant chosen so as to fit (77) to (76) at reference (no effect of drops) roughness scale: $C_s = 2.6 \cdot 10^{-13}$. Parameterizations (77) looks more attractive because concentration of sea drops should be rather defined by the wind speed at $z = A_s$ (which tears off wave crests) than u_*.

[62] The resistance law (68) with the effective roughness scale (75) and SGF specified by (76) and (77) were solved numerically by iterations. Calculations of geostrophic drag coefficient and 10-meter drag coefficient are shown in Figures 11b and 11c along with the reference (no drops) calculations and the model predictions already shown in Figures 7 and 9. If s_0 is defined by (76), the effect of drops is well pronounced (but weaker than that predicted by the model described in section 4) and results in leveling off of both C_D and C_{d10}. Note that the behavior of C_{d10} versus wind speed and magnitude of the effect is very similar to that were obtained by *Andreas* [2004] from rather different model approach based on the impact of the sea drops on momentum balance in the MABL.

[63] If s_0 is defined by (77) effect of drops is enhanced significantly. As it follows from this figure, when wind speed increases above a threshold value (60 m/s for G, and 40 m/s for u_{10}), the surface drag coefficient is rapidly reduced (crisis of the surface friction). The origin of this phenomenon is quite clear, and can be treated as a feed-back mechanism. Since spume drops generation is determined by wind speed (77) at altitude of the significant wave amplitude, suppression of surface drag results in acceleration of the airflow (similar to that shown in Figure 8), that in turn enhances drops production, that again stimulates stronger suppression of the drag and further acceleration of the wind. Thus model calculations adopting empirical data on drops concentration predict the effect comparable with the full model predictions.

[64] *Makin* [2005] assumed that at strong enough wind speed, a thin near surface layer of limited saturation (with $Ko \simeq Ko_{cr}$) by suspended droplets is generated. In some sense this assumption is similar to that shown in Figure 8c), in the narrow layer with large values of z/L the Kolmogorov number attains its critical value. However, according to the model by *Makin* [2005], such layer appears when dimensionless fall velocity $\omega = a/(\kappa u_*)$ becomes $\omega < 1$, and wind velocity and drops concentration profile inside this layer obey the asymptotic solutions (32) and (35). As discussed above, at $\omega < 1$ such asymptotic solutions are valid far from the sea surface, and unlike ''heavy'' spume drops, light drops with $\omega < 1$ cannot be confined within a thin near surface layer as they are transported upward by the turbulence.

7. Conclusion

[65] In the present paper we explored one of the possible mechanism responsible for the reduction of the sea surface drag at high winds. The mechanism is based on the direct effect of sea drops (as heavy particles) on the buoyancy force that affects the turbulent mixing. In that sense, considered mechanism is similar to that takes place in the dust storms [e.g., *Barenblat*, 1953; *Barenblat and Golitsyn*, 1974].

[66] Two cases were investigated. In the first case was assumed that the sea drops (both bubble and spume) are ejected upward from the sea surface with the rate which corresponds to the spray generation function (SGF) proposed by *Andreas* [1998]. It was found that in this case the model cannot predict any significant effect unless the SGF is enhanced in 10^3-times. Such enhancement exceeds very likely a range of uncertainty in the empirical SGF.

[67] Assumption that sea drops are ejected upward at the sea surface is only plausible for the bubble droplets. The spume droplets result from a mechanical tearing of breaking crests, and they are ejected into the airflow at altitudes of the breaking crests. To describe this phenomenon we have introduced and modeled a volume source of spume drops. According to the model, production of spume drops is defined by the total length of wave breaking crests, and the vertical profile of the volume source depends on the spectral distribution of breaking crests. The latter means the longer is the breaking wave, the higher is the altitude of the spume drops ejection. On the other hand, production of spume drops by the wind tearing from an individual breaking crest is cubic in the wind speed (that results from a thermodynamic arguments). Since the total length of breaking fronts is also proportional to the cube of the wind speed, the total volume source of spume drops is strongly wind dependent, with the wind exponent about 6.

[68] Spume drops are relatively heavy, therefore the turbulent mixing is not too efficient in their vertical distribution. The profile of spume drops concentration is defined through the balance of their tearing off from breaking crests and falling down due to the gravitation.

[69] Unlike the first case, the spume drops, being torn off from breaking crests and sprayed inside the airflow, significantly affect the turbulent mixing at strong wind speeds. The role of bubble droplets is negligible. Suppression of the turbulent mixing in the lower part of the boundary layer

leads to acceleration of the airflow and reduction of the surface drag. The effect becomes remarkable at the wind speed $u_{10} > 20$ m/s. At $u_{10} \simeq 30$ m/s the drag coefficient levels off, and then rapidly decreases at stronger wind speeds. At highest model wind speeds the model actually predicts the effect of the "slippery surface" with the drag coefficient $\sim 10^{-4}$. In overall, the model results are consistent with unique observations by *Powell et al.* [2003].

[70] Model calculations based on empirically imposed spume drops profile and rate of their generation, give the similar results that justifies essentially important impact of sea drops on the MABL and momentum exchange at the sea surface at high wind conditions. Further improvement of the model is needed. First of all, the direct effect of spume drops on the momentum balance has to be taken into account, that would allow to extend the approach to the conditions of hurricane winds of the highest force. On the other hand, the evolution of the sea drops in size due to evaporation, as well as corresponding impact on the heat balance (by means of the latent heat flux from the spray surface) can obviously affect dynamics of the atmospheric boundary layer, and thus should be further included in the model.

Appendix A: Planetary Boundary Layer (PBL)

[71] *Brown* [1982] proposed a simple model for the PBL, which consist of two layers,- the surface boundary layer (SBL) at $z < h$, and the Ekman boundary layer (EBL) at $z > h$. Inside the EBL model eddy viscosity k_h is constant and equal to the eddy viscosity in the SBL $\mathrm{k}(z)$ at its upper bound, i.e., $\mathrm{k}_h = \mathrm{k}(h)$. For the neutrally stratified EBL k_h is:

$$\mathrm{k}_h = \kappa u_* h \tag{A1}$$

The eddy-viscosity k_h defines the scale of the PBL:

$$H = \left(\frac{2\mathrm{k}_h}{f}\right)^{1/2} = 2\kappa\varepsilon\frac{u_*}{f} \tag{A2}$$

where $\varepsilon \approx 0.15$ is a tuning constant relating the SBL height h to the PBL scale H:

$$h = \varepsilon H \tag{A3}$$

In the SBL wind profile is logarithmic, and in our case is described by (64). At $z > h$ wind profile result from the solution of the Ekman equation which is:

$$\mathbf{u}(z) - \mathbf{G} = -\frac{(1-i)}{2\varepsilon}\frac{\mathbf{u}_*}{\kappa}\exp\left[-(1+i)\frac{z-h}{H}\right] \tag{A4}$$

where bold symbols denote complex variables (argument corresponds to the direction). Solution (A4) obeys continuity of the momentum flux at $z = h$.

[72] Wind profiles in the SBL (64) and EBL (A4) must be continuous at $z = h$. This condition defines the resistance law for the PBL which relates wind stress (friction velocity) to the geostrophic wind velocity:

$$\frac{\mathbf{u}_*}{\mathbf{G}} = \kappa\left[\ln\left(2\varepsilon^2\kappa\frac{u_*}{fZ_0}\right) + \frac{(1-i)}{2\varepsilon}\right]^{-1} \tag{A5}$$

[73] **Acknowledgments.** Discussion with Vladimir Makin is gratefully acknowledged. I also thank two referees for useful comments and suggestions. This investigation was supported by the Office of Naval Research (ONR) under grant N00014-03-10619 and the Norwegian Space Center under contract JOP8.3.3.06.01.2.

References

Andreas, E. L. (1992), Sea spray and the turbulent air-sea heat flux, *J. Geophys. Res.*, *97*, 11,429–11,441.
Andreas, E. L. (1998), A new spray generation function for wind speeds up to 32 m/s, *J. Phys. Oceanogr.*, *28*, 2175–2184.
Andreas, E. L. (2004), Spray stress revised, *J. Phys. Oceanogr.*, *34*, 1429–1440.
Andreas, E. L., and K. A. Emanuel (2001), Effect of sea spray on tropical cyclonic intensity, *J. Atmos. Sci.*, *58*, 3741–3751.
Andreas, E. L., J. B. Edson, E. C. Monahan, M. P. Rouault, and S. D. Smith (1995), The spray contribution to net evaporation from the sea: a review of recent progress, *Boundary Layer Meteorol.*, *72*, 3–52.
Anguelova, M., R. P. Barber, and J. Wu (1999), Spume drops produced by the wind tearing of wave crests, *J. Phys. Oceanogr.*, *29*, 1156–1165.
Bagnold, R. A. (1962), Autosuspension of transported sediment: Turbidity currents, *Proc. R. Soc. London*, *265*(315).
Banner, M. L., I. S. F. Jones, and J. C. Trinder (1989), Wavenumber spectra of short gravity waves, *J. Fluid Mech.*, *65*, 647–656.
Barenblat, G. I. (1953), On the motion of suspended particles in a turbulent flow (in Russian), *Prikl. Mat. Mekh.*, *17*, 261–274.
Barenblat, G. I., and G. S. Golitsyn (1974), Local structure of mature dust storms, *J. Atmos. Sci.*, *31*(7), 1917–1933.
Benjamin, T. B. (1959), Shearing flow over a wavy boundary, *J. Fluid Mech.*, *6*, 161–205.
Brown, R. (1982), On two-layer models and the similarity functions for the PBL, *Boundary Layer Meteorol.*, *24*, 451–463.
Donelan, M. A., J. Hamilton, and W. H. Hui (1985), Directional spectra of wave generated waves, *Philos. Trans. R. Soc. London*, *A315*, 509–562.
Donelan, M. A., B. K. Haus, N. Reul, W. J. Plant, M. Stiassnie, H. C. Graber, O. B. Brown, and E. S. Saltzman (2004), On the limiting aerodynamic roughness of the ocean in very strong winds, *Geophys. Res. Lett.*, *31*, L18306, doi:10.1029/2004GL019460.
Donnely, W. J., J. R. Carswell, and R. E. McIntosh (1999), Revised ocean backscatter model at C and Ku band under high-wind conditions, *J. Geophys. Res.*, *104*(C5), 11,485–11,497.
Dulov, V., V. Kudryavtsev, and A. Bol'shakov (2002), A field study of white caps coverage and its modulations by energy containing waves, in *Gas Transfer at the Water Surface*, edited by M. A. Donelan et al., pp. 187–192, AGU, Washington, D. C.
Emanuel, K. A. (1995), Sensitivity of tropical cyclones to surface exchange co-efficients and a revised steady-state model incorporating eye dynamics, *J. Atmos. Sci.*, *52*, 3969–3976.
Iida, N., Y. Toba, and M. Chaen (1992), A new expression for the production rate of sea water droplets on the sea surface, *J. Phys. Oceanogr.*, *22*, 439–460.
Kaplan, J., and W. M. Frank (1993), The large scale inflow-layer structure of Hurricane Frederic (1979), *Mon. Weather Rev.*, *121*, 3–20.
Kazanski, A. B., and A. S. Monin (1961), On the dynamic interaction between the atmosphere and earth surface (in Russian), *Izv. Akad. Nauk SSSR, Geophys. Ser.*, *5*, 514–515.
Kolmogorov, A. N. (1954), On a new variant of the gravitational theory of motion of suspended sediments (in Russian), *Izv. Akad. Nauk SSSR, Phys. Ser.*, *6*, 56–58.
Kudryavtsev, V. N., and V. K. Makin (2001), The impact of air-flow separation on the drag of the sea surface, *Boundary Layer Meteorol.*, *98*, 155–171.
Kudryavtsev, V. N., and V. K. Makin (2004), Impact of swell on marine atmospheric boundary layer, *J. Phys. Oceanogr.*, *34*(4), 934–946.
Longuet-Higgins, M. S. (1957), The statistical analysis of a random moving surface, *Philos. Trans. R. Soc. London*, *A249*, 321–387.
Longuet-Higgins, M. S. (1978), The instability of gravity waves on deep water. I. Superharmonics, *Proc. R. Soc. London*, *A360*, 471–488.
Makin, V. K. (1998), Air-sea exchange of heat in the presence of wind waves and spray, *J. Geophys. Res.*, *103*(C1), 1137–1182.
Makin, V. K. (2005), A note on drag of the sea surface at hurricane winds, *Boundary Layer Meteorol.*, *115*(1).
Melville, K., and P. Matusov (2002), Distribution of breaking waves at the ocean surface, *Nature*, *417*, 58–63.
Monahan, E. C. (1986), The ocean as a source for atmospheric particles, in *The Role of Air-Sea Exchange in Geochemical Cycling*, edited by P. Buat-Menart, pp. 129–163, Springer, New York.

Monin, A. S., and A. M. Yaglom (1965), *Statistical Fluid Mechanics*, vol. 1, Nauka, Moscow. (English translation, MIT Press, Cambridge, Mass., 1971.)
Phillips, O. M. (1985), Spectral and statistical properties of the equilibrium range in wind-generated gravity waves, *J. Fluid Mech.*, *156*, 505–530.
Plant, W. J. (1982), A relationship between wind stress and wave slope, *J. Geophys. Res.*, *87*, 1961–1967.
Powell, M., P. Vickery, and T. Reinhold (2003), Reduced drag coefficient for high wind speeds in tropical cyclones, *Nature*, *422*, 279–483.
Prandtl, L. (1949), *Fuhrer durch die Stromungslehre*, 3rd ed., F. Vieweg, Braunschweig.
Reul, N., H. Branger, and J.-P. Giovanangeli (1999), Air flow separation over unsteady breaking waves, *Phys. Fluids*, *11*, 1959–1961.
Smith, M. H., P. M. Park, and I. Consterdine (1993), Aerosol concentration and estimated flux over the sea, *Q. J. R. Meteorol. Soc.*, *119*, 809–824.
Sullivan, P., J. McWilliams, and C.-H. Moeng (2000), Simulation of turbulent flow over idealized water waves, *J. Fluid Mech.*, *404*, 47–85.
Toba, Y. (1973), Local balance in the air-sea boundary processes III: On the spectrum of wind waves, *J. Oceanogr. Soc. Jpn.*, *29*, 209–220.
Wu, J. (1993), Production of spume drops by the wind tearing of wave crests: The search for quantification, *J. Geophys. Res.*, *98*, 18,223–19,221.

V. N. Kudryavtsev, Nansen International Environmental and Remote Sensing Center, 26/28, Bol'shaya Monetnaya, Saint-Petersburg 197101, Russia. (vladimir.kudryavtsev@niersc.spb.ru)